SCIENCE AND TECHNOLOGY ORGANIZATION
CENTRE FOR MARITIME RESEARCH AND EXPERIMENTATION

Reprint Series **CMRE-PR-2019-104**

Assessment of sea wave spectra using a surfaced glider

Alberto Alvarez

June 2019

Originally published in:

Deep Sea Research Part I: Oceanographic Research Papers, volume 102, August 2015, pp. 135-143, doi: doi.org/10.1016/j.dsr.2015.04.015

About CMRE

The Centre for Maritime Research and Experimentation (CMRE) is a world-class NATO scientific research and experimentation facility located in La Spezia, Italy.

The CMRE was established by the North Atlantic Council on 1 July 2012 as part of the NATO Science & Technology Organization. The CMRE and its predecessors have served NATO for over 50 years as the SACLANT Anti-Submarine Warfare Centre, SACLANT Undersea Research Centre, NATO Undersea Research Centre (NURC) and now as part of the Science & Technology Organization.

CMRE conducts state-of-the-art scientific research and experimentation ranging from concept development to prototype demonstration in an operational environment and has produced leaders in ocean science, modelling and simulation, acoustics and other disciplines, as well as producing critical results and understanding that have been built into the operational concepts of NATO and the nations.

CMRE conducts hands-on scientific and engineering research for the direct benefit of its NATO Customers. It operates two research vessels that enable science and technology solutions to be explored and exploited at sea. The largest of these vessels, the NRV Alliance, is a global class vessel that is acoustically extremely quiet.

CMRE is a leading example of enabling nations to work more effectively and efficiently together by prioritizing national needs, focusing on research and technology challenges, both in and out of the maritime environment, through the collective Power of its world-class scientists, engineers, and specialized laboratories in collaboration with the many partners in and out of the scientific domain.

NOTE: The CMRE Reprint series reprints papers and articles published by CMRE authors in the open literature as an effort to widely disseminate CMRE products. Users are encouraged to cite the original article where possible.

Deep-Sea Research I

journal homepage: www.elsevier.com/locate/dsri

Instruments and Methods

Assessment of sea wave spectra using a surfaced glider

A. Alvarez *

NATO-STO Center for Maritime Research and Experimentation-CMRE, La Spezia, Italy

ARTICLE INFO

Article history:
Received 12 November 2014
Received in revised form
17 March 2015
Accepted 28 April 2015
Available online 9 May 2015

Keywords:
Underwater glider
Response amplitude operator
Waverider buoy analogy
Accelerometer
Non-directional and directional sea wave spectra

ABSTRACT

The determination of non-directional and directional sea wave spectra is attempted by analyzing the dynamical response of a surfaced Slocum glider. The method makes use of the glider heave motion to infer non-directional properties of the wave spectra. In addition, surge and sway motions are considered to derive wave directionality. The transfer functions for heave, surge and sway for a surfaced Slocum glider has been computed to determine the impact of the body geometry/inertia and the angle of incidence on the response of the surfaced platform when excited by regular waves. Numerical results show that for wave periods longer than 6 s, motions measured at the glider platform can be assumed equivalent to motions experimented by the water parcels at the sea surface. Spectral information about sea state conditions can then be directly derived from the measurement of glider responses. Results also reveal a natural period of the surfaced glider at around 5 s. A series of field experiments were conducted during March 7th, May 17th and May 27th of 2013 in a marine region off-shore La Spezia, to validate the methodology. Specifically, the wave spectra derived from a Slocum glider equipped with a set of accelerometers was compared against the values provided by a Datawell Waverider Mk3 moored in the vicinity of the glider deployment. Agreement has been found between the non-directional estimates from the glider and the values measured by the waverider. Regarding wave directionality, glider estimates of peak direction agree well with those reported by the waverider. More significant differences are found between the directional spread estimates.

1. Introduction

Surface wave processes are mainly generated at the ocean's surface due to the interaction with the atmosphere immediately above it. These are usually characterized by wavelengths and amplitudes ranging from centimeters up to hundreds of meters and from millimeters up to tens of meters, respectively. Ocean waves have an enormous impact on ocean physical processes and human related activities. They significantly influence air–sea fluxes by determining the drag at sea surface (Sullivan and McWilliams, 2010), increase turbulent mixing in ocean's upper layer (Sutherland et al., 2013; D'Asaro et al., 2013), modify the bottom friction coefficient for ocean currents (Wolf and Prandle, 1999), generate rip currents (Yu, 2006) and modify the sediment transport conditions and erosion in nearshore regions (Komar, 1998; Hsu et al., 2006). Sea state conditions are of central importance for maritime structures (Goda, 2010), maritime transport (Vanem and Bitner-Gregersen, 2012) and search and rescue (Bezgodov and Esin, 2014) among others.

Despite the different technologies developed to monitor sea state conditions, wave observations still remain sparse relative to the size of oceans. These are predominantly provided by waverider buoys and remote sensing. The former is a buoy moored to the sea bottom by means of an elastic mooring in order to follow the sea surface (Tucker and Pitt, 2001). The buoy is instrumented with an accelerometer that registers the rate at which the buoy is rising or falling as it follows the wave pattern. Vertical displacements are then derived from the sampled vertical accelerations (Earle, 1996; Niclasen and Simonsen, 2007). A limited number of waverider buoys also record pitch, roll and accelerations in the horizontal axes to derive directional properties of the incident wave field.

Remote sensing offers alternative procedures to complement *in situ* observations. High frequency (HF) radars have been extensively used to extract information about ocean waves from the sea echo spectrum. This is achieved by inversion techniques based on empirical or physically-based models relating the radar backscatter spectrum to the ocean wave spectrum (Graber and Heron, 1997). Information about wave height is also obtained by radar altimeters (Queffeulou, 1987) and synthetic aperture radars (SAR) aboard low-orbiting satellites (Swift and Wilson, 1979;

* Correspondence to: CMRE, Viale San Bartolomeo 400, 19126 La Spezia, Italy. Tel.: +39 187 527298.
E-mail address: Alberto.Alvarez@cmre.nato.int

http://dx.doi.org/10.1016/j.dsr.2015.04.015
0967-0637/

Heimbach et al., 1998; Alpers, 2003). The former infers the roughness of the ocean surface from the shape of the return pulse while the latter make use of the modulation that ocean waves generate in the backscatter of microwaves from the sea surface. The SAR sensor is able to provide images from the sea surface with sufficient resolution to detect surface wave processes (Kanevsky, 2009). Ocean wave fields have been measured remotely by Hwang et al. (2000), Reineman et al. (2009) and Romero and Melville (2010) using light detection and ranging (lidar) systems onboard airplanes. Airborne lidar provides spatiotemporal measurements of waves accurate enough to allow *in situ* calibration of marine-radar-based measurements of sea state.

Other procedures to measure sea state conditions exist, but their application is less extended. Shipborne wave recorders are among them (Tucker and Pitt, 2001). These are constituted by a set of accelerometers and pressure sensors distributed at different ship locations. Accelerometers measure vertical movements induced by the waves while pressure records are used to correct the effects of ship geometry and inertia (in general, ships do not accurately follow the sea surface). Shipborne sensors provide *in situ* observations in open seas where the coverage of waverider buoys or HF radars is very limited or non-existent.

Recent technological developments on autonomous vehicles may expand the capabilities to provide sea state observations as an added value. For example, an unmanned surface vehicle (wave glider) was recently used by Lenain and Melville (2014) to record different oceanographic (including sea state) and atmospheric variables as the platform passed near the category 3 Tropical Cyclone Freda. Goodman et al. (2010) estimated surface wave displacements from motion and pressure sensors onboard a moving autonomous underwater vehicle-AUV. Underwater gliders are other unmanned platforms that are becoming popular in oceanography. These are autonomous vehicles designed to observe vast areas of the interior ocean (Stommel, 1989). For this reason, there is a significant growing interest in glider technology by oceanographers (Testor et al., 2009). Making use of buoyancy changes, their hydrodynamic shape and small wings, gliders carry out undulatory motions between the surface and a pre-determined depth, with a net horizontal displacement with a speed of about 1 km/h. Gliders have an endurance of one to several months, covering distances of thousand kilometers (recently, a glider crossed the Atlantic Ocean ($\sim$5300 km) in a 7 month mission; Shapiro, 2010). During a mission, a glider periodically surfaces to re-position and establish communications with the base station. The time at surface is programmable and it usually ranges from few minutes up to an hour depending on the amount of information to be transmitted. This working procedure suggests the possibility to expand the sensing capabilities of the glider platform to provide also information about present sea state conditions.

Non-directional wave spectrum refers to the vertical fluctuations of the water surface at a fixed location and thus, only the raise and fall motion of the water surface is needed for its estimation. As it was previously mentioned, a popular and widely used method to derive non-directional waves is measuring the heave motion of a body (*i.e.* a buoy), and then converting the body's heave into wave vertical motion by means of the body's heave response function (Chen-Tung, 2009; Holthuijsen, 2010). By using this approach, non-directional wave parameters have been obtained by Pereira and Sukhatme (2010) from glider vertical motions measured by an on-board accelerometer and assuming that the glider follows the sea surface (hereinafter referred as the waverider buoy analogy). Their scope was to predict glider communication quality. Although sharing similar trends, discrepancies were found between the sea surface height derived from the glider and a reference waverider buoy. These differences were justified in terms of the large distance (25 km) between the locations of the glider surfaces and the waverider buoy. This prevented a clear assessment of the methodology and, up to author's knowledge, the validation of the waverider buoy analogy for a surfaced glider is still an open issue. Mathematically, the assumption holds if the complex valued transfer function, that relates the measured glider response to the wave energy spectrum, equals to one for the frequency range of typical sea waves. Otherwise, the transfer function must be taken into account in order to correct the effects in the dynamical response of the body geometry and inertia as well as the wave angle of incidence.

The directional sea spectrum provides the energy distribution in terms of frequencies and directions of incidence of waves. In addition to the heave motion, other motions are required to derive information about wave directionality from the motion of a floating body. For example, the so called particle-following technique makes use of body's heave, surge and sway motions to estimate wave directionality (Young, 1999). Again, response functions of these motions are used to convert body's to wave motions. Directional wave information is then obtained from a cross-spectral analysis among the heave motion and the other two orthogonal motions. Similarly to the non-directional case, body's motions are equivalent to wave motions if the waverider buoy analogy holds.

This study further investigates, in general, the capability of underwater glider technology to provide non-directional and directional properties of sea state conditions and, in particular, the validity of the waverider buoy analogy for a surfaced glider. This is done first by the numerical determination and analysis of the transfer function for heave, surge and sway motions of a surfaced glider excited by regular waves and second, by experimental comparison of the non-directional and directional wave spectrum provided by a waverider buoy with the spectrum estimated from a surfaced glider assuming the waverider buoy analogy. The study has been done using a Slocum glider (Webb Res. Co.-Teledyne, Falmouth-MA; Webb et al., 2001) which is operated by many users worldwide, including CMRE. This facilitates direct exploitation by other users of the results derived from this study. On the other hand, the application of the described methodology to other gliders would be straightforward. The article is organized as follows: Section 2 describes the methodology followed to numerically compute the transfer function for heave of a surfaced glider as well as the experimental set up done to assess the non-directional and directional sea spectra from a surfaced glider. Numerical and experimental results are presented in Section 3. Finally, Section 4 discusses and concludes the work.

2. Model and data

2.1. Model of the transfer functions of a Slocum glider excited by regular waves

The main objective of this subsection is to determine the frequency characteristics of the responses of a surfaced glider when excited by waves. This is because for small glider motions, the statistics of the responses obtained from measuring glider motions can be converted to wave energy spectra if the response spectra of the glider are known. To do that, a free-floating Slocum glider is assumed at the sea surface (Fig. 1). The glider has a hull length of 1.79 m and a diameter of 0.213 m. This hull is formed by a frontal ellipsoidal section of 0.21 m length, a central cylindrical part of 1.21 m and second ellipsoidal portion of 0.37 m at the rear part of the body. At the sea surface, the platform gets a pitch of 10° to position antennae (located at the rear part of the vehicle) out of water. The wings, located at 0.76 m from the nose, have a total surface of 0.0972 m^2, a wing span of 0.99 m and a thickness of 0.002 m. Their tip and hull chords are 0.145 and 0.11 m,

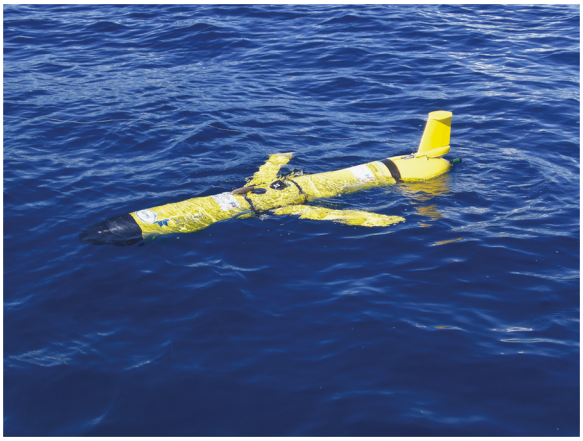

Fig. 1. A surfaced Slocum glider.

respectively. The wing has swept angles of 0.77 rad and 0.72 rad at the leading and trailing edges.

The surfaced glider interacts with a regular wave field consisting of a prescribed incident wave system plus outgoing waves associated with the radiation and scattering. Hydrodynamic pressures are generated on the surface of the glider as a result of the interaction with the wave field. Integration of these pressures provides the hydrodynamic forces and moments acting on the body. If the wave steepness (*i.e.* ratio between the wave height and the wavelength) is small, the free surface and body boundary conditions can be linearized around their mean positions to determine these pressure fields. A time-harmonic dependence in the oscillatory motions of the floating body is also assumed. Under this linearization and time dependence, the resulting motion of a body in waves can be seen as a superposition of the motion of the body in still water and the forces on the restrained body in waves (Newman, 1977). The former defines the so-called hydromechanical forces and moments which described the bulk effect of pressure forces on the body exerted by its oscillating motion in the undisturbed surface of the fluid. The latter are the so-called wave exciting forces and moments which are the forces generated by the incident and scattered waves on the restrained body. Physically, hydromechanical loads are expressed in terms of a potential mass and damping of the body's motion, while exciting forces are represented by an external forcing of the body's oscillation. Thus, the small body motions on the different degrees of freedom are dynamically described by a system of damped and coupled harmonic oscillators subjected to external forcing (Newman, 1977):

$$(M_{ij}+A_{ij})\ddot{\eta}_j+B_{ij}\dot{\eta}_j+C_{ij}\eta_j=F_i e^{i\omega t} \tag{1}$$

where η_i, $i=1\ldots3$ represent the amplitudes of translation displacements in the x, y and z directions (surge, sway and heave, respectively) while η_i, $i=4\ldots6$ are the amplitudes of rotational displacements about the same axis (roll, pitch and yaw, respectively). These displacements are represented on a right handed Cartesian coordinate system, fixed with respect to the mean position of the body and with the origin in the plane of the undisturbed free surface. The terms M_{ij}, A_{ij}, B_{ij} and C_{ij} are the mass-inertia matrix of the body, the matrix of added mass coefficients, the damping coefficient matrix and the hydrostatic restoring terms, respectively. Finally, F_i represents the complex amplitude of the exciting force in the ith direction. The responses of a surfaced glider when excited by a given regular wave field can be determined once these terms are known. Coefficients in matrices M_{ij} and C_{ij} can be computed knowing the shape and internal mass distribution of the floating body, whereas, matrices A_{ij} and B_{ij} describe the hydromechanical loads. Their coefficients are usually estimated considering that the fluid is homogeneous, inviscid and incompressible and the fluid motion is irrotational. These assumptions on the physical nature of the fluid define the framework of potential flow solvers, which are used almost exclusively in seakeeping calculations and have been successfully employed to investigate the hydrodynamics of underwater gliders (Alvarez, 2010). Potential flow methods are fast and simple in terms of grid generation as they need only to discretize the boundaries of the domain instead the whole fluid space (Bertram, 2011). The validity and implications of considering a potential flow in the present study will be discussed in Section 4.

Hydromechanical loads, A_{ij} and B_{ij}, and exciting forces, F_i, are computed in the potential flow framework by assuming that the flow velocity is given in terms of a velocity potential:

$$\Phi(x,y,z,t)=\mathrm{Re}\left(\varphi(x,y,z)e^{i\omega t}\right) \tag{2}$$

The time independent velocity potential can be decomposed as (Newman, 1977):

$$\varphi(x,y,z)=i\omega\sum_{j=1}^{6}\eta_j\varphi_j(x,y,z)+A(\varphi_I+\varphi_S) \tag{3}$$

where ϕ_j (jth radiation potential) is the time independent velocity potential corresponding to an oscillation of the body with unit amplitude and in the jth direction, $\varphi_I=i\frac{g}{\omega}e^{kz}e^{-ik(x\cos(\theta)+y\sin(\theta))+i\omega t}$ is the velocity potential of the incident wave with unit amplitude, k is the wave-number, g is the acceleration of gravity, θ is the angle of incidence of the wave, ϕ_s is the scattered potential and A is the amplitude of the incident wave. The complex spatial part of the velocity potentials must satisfy (Newman, 1977):

$$\begin{aligned}
&\nabla^2\phi_{j,S}=0, \text{continuity condition of the velocity field,}\\
&\tfrac{\partial\phi_{j,S}}{\partial z}-K\phi_{j,S}=0 \quad \text{for } z=0, \text{ free surface boundary condition,}\\
&\tfrac{\partial\phi_{j,S}}{\partial z}\to 0 \text{ as } z\to-\infty, \text{sea bottom boundary condition,}\\
&\tfrac{\partial}{\partial n}(\phi_I+\phi_S)=0, \quad \text{kinematic boundary condition on body surface,}\\
&\tfrac{\partial}{\partial n}\phi_j=n_j,\ j=1\ldots6, \text{ kinematic boundary condition on body surface, and}\\
&\sqrt{R}\{\tfrac{\partial}{\partial R}-iK\}\phi_{j,S}\to 0 \text{ when } R\to\infty,\ z\le 0, \text{ and } R=\sqrt{x^2+y^2}, \text{ radiation condition}
\end{aligned} \tag{4}$$

where $K=\omega^2/g$, $(n_1, n_2, n_3)=(n_x, n_y, n_z)$ are the components of a unit vector normal to the body surface (outward of the fluid) and $(n_4, n_5, n_6)=(x, y, z)\times(n_x, n_y, n_z)$. The boundary value problem Eq. (4) is solved by using the Green's theorem to derive integral equations for the different velocity potentials on the body boundary. The integral equation satisfied by the radiation velocity potentials ϕ_j on the body boundary is:

$$\begin{aligned}
&2\pi\varphi_j\left(\vec{x}\right)+\iint_S\varphi_j\left(\vec{\xi}\right)\frac{\partial G\left(\vec{x};\vec{\xi}\right)}{\partial n_\xi}dS\\
&\quad=\iint_S n_j G\left(\vec{x};\vec{\xi}\right)\ \mathrm{dS}\ ,\ \left\{\vec{x},\vec{\xi}\right\}\in \text{ body surface}
\end{aligned} \tag{5}$$

where S denotes the body wetted surface at calm water and $G\left(\vec{x};\vec{\xi}\right)$ is the Green function or influence function of a pulsating source located at $\vec{\xi}\equiv\left[\xi_x,\xi_y,\xi_z\right]$ on the potential ϕ_j at location $\vec{x}\equiv[x,y,z]$. The Green function satisfies the Laplace equation, the linearized boundary conditions at the sea surface and the radiation condition at infinity. Its mathematical expression is given by (Wehausen and Laitone, 1960):

$$\begin{aligned}
G\left(x,y,z;\xi_x,\xi_y,\xi_z\right)&=\tfrac{1}{r}+\tfrac{1}{r'}+2K(P.V.)\int_0^\infty\tfrac{1}{k-K}e^{k(z+\xi_z)}J_0(kR)dk\\
&\quad-2\pi iKe^{K(z+\xi_z)}J_0(KR),
\end{aligned}$$

$$r=\sqrt{(x-\xi_x)^2+\left(y-\xi_y\right)^2+(z-\xi_z)^2},$$
$$r'=\sqrt{(x-\xi_x)^2+\left(y-\xi_y\right)^2+(z+\xi_z)^2},$$
$$R=\sqrt{(x-\xi_x)^2+\left(y-\xi_y\right)^2}, \quad (6)$$

where P.V. and $J_0(.)$ refer to the Principal Value of the integral and the Bessel function of zero order. For finite water depth D, Eq. (6) is valid as long as $\tanh(kD)\sim 1$ (deep water waves). The coefficients of matrix A_{ij} and B_{ij} are then derived from the radiation potentials ϕ_j by solving the equation (Newman, 1977):

$$A_{ij}-\frac{i}{\omega}B_{ij}=\rho\iint_S n_i\phi_j dS, \quad (7)$$

with ρ being the density of the fluid. Instead, the exciting forces can be computed using the Haskind relations (Newman, 1977):

$$F_i=-i\omega\rho\iint_S\left(n_i\phi_I-\phi_i\frac{\partial\varphi_I}{\partial n}\right)dS, \quad (8)$$

Resolution of Eq. (5) must be done numerically in most cases. In this work, the boundary integral equation method (BIEM) described in Lee and Newman (2004) was programmed in Matlab for this purpose (Alvarez, 2012). Specifically, the body surface is segmented into N small triangular or quadrilateral panels $\{S_k\}$. Eq. (5) is then discretized by collocation on the coordinates of each panel centroid $\{x_k\}$, $k=1\ldots N$. The integral is carried out by the summation over the corresponding integrals over each panel, evaluated using a fourth order Gaussian quadrature. Discretization of Eq. (5) takes then the form of a system of N equations with N unknowns:

$$2\pi\phi_j\left(\vec{x}_n\right)+\sum_{k=1}^{N}M_{nk}\phi_j\left(\vec{x}_k\right)=\sum_{k=1}^{N}G_{nk}n_j\left(\vec{x}_k\right), \quad n=1\ldots\mathrm{N}$$
$$M_{nk}=\iint_{S_k}\frac{\partial G\left(\vec{x}_n;\vec{\xi}\right)}{\partial n_\xi}dS_k,$$
$$G_{nk}=\iint_{S_k}G\left(\vec{x}_n;\vec{\xi}\right)dS_k, \quad \vec{\xi}\in k\text{ th panel } S_k \quad (9)$$

For each collocation and field point, the Green function Eq. (6) is computed using a recursive adaptive Simpson quadrature and isolating the singularity of the integrand. Notice that faster algorithms can be implemented to compute the Green function (Teslen and Noblesse, 1986). The numerical approach has been completed by using the extended boundary condition method (EBCM) (Lee and Scalvounonos, 1989) to prevent solutions to suffer from the effect of irregular frequencies that may appear due to the ill-condition of the resulting linear system of equations at some discrete frequencies (usually this effect appears at frequencies higher than the frequency range of typical sea spectra). The matrix of added mass coefficients, the damping coefficient matrix and the exciting forces are derived from the discretized radiation potentials obtained from Eq. (9). Validation of the numerical approach is provided in Alvarez (2012).

Once the terms M_{ij}, A_{ij}, B_{ij}, C_{ij} and F_i are computed, Eq. (1) can be used to determine the frequency characteristics of the responses of a floating body (in the present case a glider) when excited by regular waves at different frequencies and incident directions. Specifically, Eq. (1) is written in the frequency domain like:

$$\left[-\omega^2(M_{ij}+A_{ij})+i\omega B_{ij}+C_{ij}\right]\widehat{\eta}_j=F_i \;;\quad \eta_j=\widehat{\eta}_j e^{i\omega t}, \quad (10)$$

The solutions of the system of equations are the transfer functions for the responses, $H_j(\omega,\theta)=(\widehat{\eta}_j(\omega,\theta)/A)$, and the response amplitude operator (RAO) is the magnitude of the transfer function. Transfer functions represent a linear approximation of the frequency response of the body motion in regular waves. Notice that if the scale of the body is small relative to the wave length (as it generally occurs for glider platforms), $H_j(\omega,\theta)$ is expected to be close to one for the displacements orthogonal to the wave front. Non-directional and directional spectral information about sea state conditions can then be directly derived from measurements of the response of the body in suitable degrees of freedom (Chen-Tung, 2009; Holthuijsen, 2010).

2.2. Data

A shallow water Slocum glider was modified to host on board a sensor package, associated data logger, batteries and control unit, to record the platform motions when she is at the surface. The sensor package PhidgetSpatial 3/3/3 comprises a 6-axis inertial measurement unit (IMU) that measures accelerations up to $\pm 5g$ with a resolution of 976 μg and a precision of 2.8 mg (the resolution and precision are enhanced to 76.3 μg and 280 μg, respectively, when measuring less than $\pm 2g$), and angular rotations up to $\pm 400^\circ$ per second in 3-axis with a resolution of 0.07° per second and a precision of 0.59° per second. The sensor package also includes a compass that measures magnetic fields up to ± 4 Gauss in the same axes, with a resolution of 3 mG and a precision of 1.2 mG. The body-fixed axes defined by the IMU sensor were given with the positive x, y and z axes in the bow, starboard and downward directions, respectively. A clock was also included to provide an approximate absolute time reference (month/day/hour/minute/seconds) to the samples. The package was located close to the center of gravity of the platform.

An experiment named Marine Environmental Radar and Glider Experiment 2013 (MERGE 13) was conducted with the modified Slocum glider on March 7th, May 17th and May 27th in the Ligurian Sea off the island Isola Palmaria, Fig. 2. Specifically, the glider was deployed in the vicinity of a Datawell Waverider Mk3 (Datawell, 2006) moored at 9.816° longitude and 44.033° latitude in a 29 m water depth. Data from the waverider provided the ground truth conditions to compare with the glider. Glider deployments were done under rough seas and never farther than 900 m from the waverider (although this distance was later

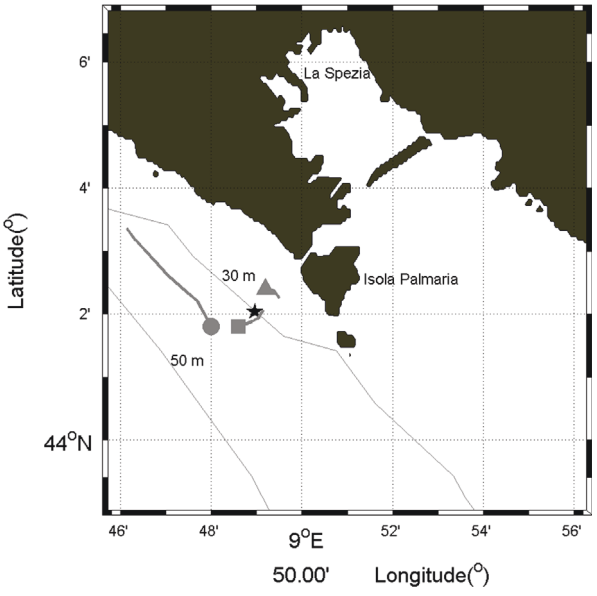

Fig. 2. Glider deployments during March 7th (gray circle), March 17th (gray triangle) and March 27th (gray square) of 2013. Grey lines represent the drifting trajectories during the data collection period. The location of the Datawell Waverider Mk3 is respresented by the black star.

Table 1
Sea state conditions obtained from the waverider during the three deployments.

Date	Peak period (s)	Mean period (s)	Wavelength (m)	Depth (m) at deployment location	Tanh (*kD*)
May 7th	8.33	6.04	106.4	40	0.982
May 17th	6.17	5.2	58	20	0.974
May 27th	6.57	5.06	67	37	0.997

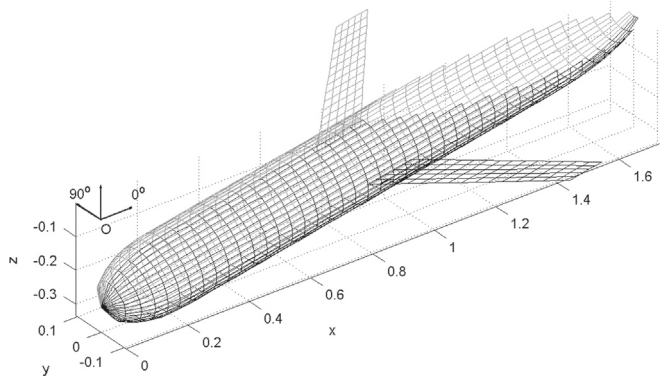

Fig. 3. Semi-submerged glider configuration and definition of sea directions used in the numerical computation of response functions. Point *O* is the origin of the coordinate system.

exceeded in some cases due to the drift of the glider at the sea surface). The water depth at the glider deployment location was between 20 and 40 m verifying that $0.97 < \tanh(kD) < 1$. This justifies the use of Eq. (6) for the sea state conditions found in the three deployments (Table 1). The glider remained at the sea surface recording information for an hour during each deployment. Accelerations, angular rotations and magnetic fluxes from the PhidgetSpatial 3/3/3 were acquired every 16 ms. Records were segmented into 30 min portions during an hour sampling period to match the 30-min measurement cycles of the Datawell Waverider Mk3 (Datawell, 2006).

3. Results

3.1. Numerical transfer functions of a surfaced Slocum glider

The heave, surge and sway response functions of a surfaced Slocum glider were computed using the theoretical framework reported in Section 2. As it was previously mentioned, heave was selected because it is the variable mostly used by *in situ* wave measurement systems to infer non-directional sea wave spectra. It also shows the advantage that, as it is shown below, its response function for the glider geometry does not depend on the direction of incidence of long waves. Surge and sway motions were considered to apply the particle-following principle used by the Datawell Waverider Mk3 to estimate directional wave properties (Datawell, 2006).

To proceed with the numerical computation, the hull of a Slocum glider was segmented into 742 panels, Fig. 3. Notice that only the submerged portion of the hull in its mean position at the sea surface is considered in the computations. This is because only the wetted surface of the body is subjected to fluid pressures, and because boundary conditions at the sea surface and body hull are

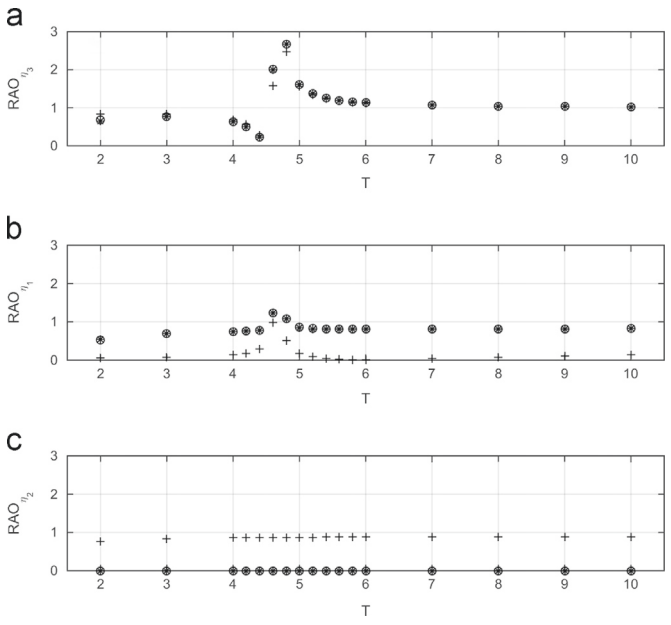

Fig. 4. RAO for heave (a), surge (b) and sway (c) for sea directions of 0° (o), 90° (+) and 180° (*). T is the wave period in seconds.

linearized around their mean positions. Wings have been modelled by plates of 0.002 m thickness.

Fig. 4 show the RAO for heave, surge and sway motions for different wave periods and sea directions. Regarding heave, results show the existence of a resonance marked in the diagrams by a local maximum in the RAO (Fig. 4a). Analytical approximations of a coupled heave-pitch dynamical model of the case under study, corroborates the existence of resonance phenomena at 4.8 s which corresponds to the natural frequency of the surfaced platform. The RAO decreases for small wave periods while it is close to 1 for wave periods longer than 6 s. For wave periods equal or longer than 6 s the glider behaves as a small body, following the wave surface. In this case, vertical accelerations measured at the glider platform can be assumed equivalent to the vertical accelerations experimented by the water parcels at the sea surface.

Unlike for heave motion, RAOs for surge and sway strongly depend on the direction of incidence of the wave, Fig. 4b and c. The RAO is zero for a displacement along the wave front, and close to one when it is perpendicular and for wave periods longer than 6 s. This agrees with the horizontal displacement of water parcels which motions are in a plane determined by the wave vector and the vertical direction. No wave signal is found in the horizontal direction orthogonal to that plane. Thus, the waverider buoy analogy is also expected to be a good approximation to determine directional wave spectrum for wave periods longer than 6 s. Notice that no resonance is found for sway motions because this mode is uncoupled with heave and pitch for the glider geometry. This is not the case for surge motions.

3.2. Validation of non-directional spectra derived from surfaced glider responses

Based on the wave conditions found during the field trials (Table 1) and the numerical results of the previous sub-section, a data processing sequence along the lines described by Earle (1996) was implemented post deployment to assess the variance spectrum from the recorded glider vertical accelerations. Specifically, data were resampled at 4 Hz which corresponds to the rounded value of the sampling frequency of the Datawell Waverider Mk3 (3.84 Hz; Datawell, 2006) and the 30 min record was further

subdivided into segments of 300 s. This segment length was selected because, for the mean periods of around 6 s found during the trials (see Table 1), a total number of 50 wave cycles was expected on each segment. According to the 17th International Towing Tank Conference –ITTC84 (ITTC, 1984), this is the lower limit of cycles suggested to obtain proper spectral shapes and statistical values from irregular wave measurements. Next, the mean value was removed from each segment. A spectral leakage reduction was done for each segment using a Hanning window:

$$W(n\Delta t) = \frac{1}{2}\left(1 - \cos\left(\frac{2\pi n}{L}\right)\right), \quad 0 \le n \le L-1 \tag{11}$$

where L is the length of each data segment. The Power Spectral Density (PSD) of vertical acceleration was then computed using a Fast Fourier Transform. At the low frequency end, accelerations become very small and disappear in the sensor noise. This low frequency noise is due to drifts in the accelerometer's zero stability and due to lower frequency tilts of the platform which changes the component of gravitational acceleration. A digital high-pass filter with cut offs at 16 s for March 7th and 12 s for May 17th and May 27th were applied when computing the PSD. The cut offs were fixed by determining the frequency at the low frequency end, where the unfiltered PSD starts to rise by the prevailing low frequency variance. The final PSD is obtained as the average of the spectral densities obtained for the different segments. During half an hour, a total of 12 spectra of 300 s data interval are averaged. This is comparable to the number of spectra realizations, eight, employed by the Datawell (2006) Waverider.

The PSD of vertical acceleration is transformed into a PSD of vertical motion in the frequency space by the transformation:

$$E_z(\omega) = \frac{E_{a_z}(\omega)}{\omega^4} \tag{12}$$

where ω is the angular frequency and E_{az} (.) and E_z(.) are the PSD of vertical accelerations and displacements, respectively. Standard parameters like the significant wave height (H_s), mean period (T_1) and zero up-cross periods (T_2) are computed from the nth-order moments of the area under the spectrum defined in Eq. (12) with respect to the vertical axis at zero frequency (Earle, 1996):

$$m_n = \int_0^\infty \omega^n E_z(\omega) d\omega \tag{13}$$

where m_n is the nth moment. Parameters H_s, T_1, T_2 and T_p (period of the component with highest spectral density) derived from glider records were selected for validation against the values provided by the Datawell Waverider Mk3.

Results obtained from the processing of vertical accelerations during the different tests are summarized in Figs. 5–7. Specifically, they display the PSD of vertical displacements (heave motion) computed from the history of vertical accelerations following the procedure described previously. The PSD derived from glider measurements is compared in each figure with the PSD obtained from the Datawell Waverider Mk3 (Datawell, 2006) for the same period of time. In general, the figures qualitatively show a good agreement between the PSD derived from both platforms at the frequency band of interest. Certain discrepancies are observed between both PSDs near the low-frequency cut-off. These discrepancies are likely induced by differences in the signal processing methodology to filter out low-frequencies with poor signal to noise ratio. Table 2 compares the value of the parameters H_s, T_1, T_2 and T_p derived from the glider motion at sea surface with those values obtained from the Datawell Waverider Mk3 for the three deployments. For all parameters and deployments, the differences are within 15% of the estimated value. These results confirm the initial hypothesis that non-directional sea state parameters could also be provided by glider platforms.

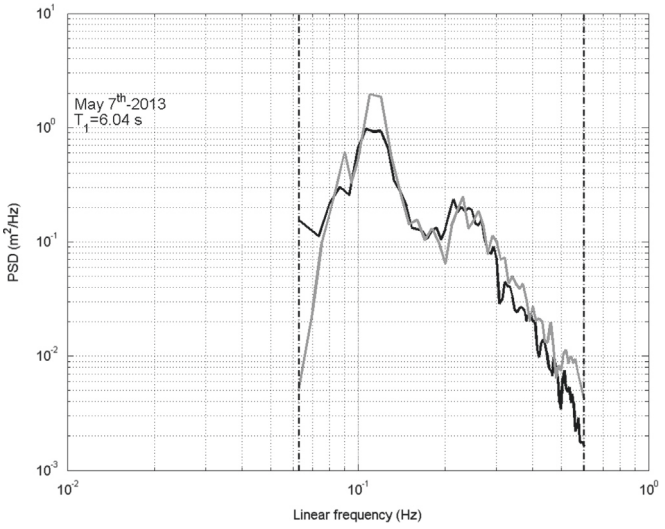

Fig. 5. Power spectral density of the wave field computed from the glider response (black solid line) and from the waverider (gray solid line) during March 7th. Dashed solid lines indicate the frequency cut-offs. T_1 is the mean period provided by the waverider.

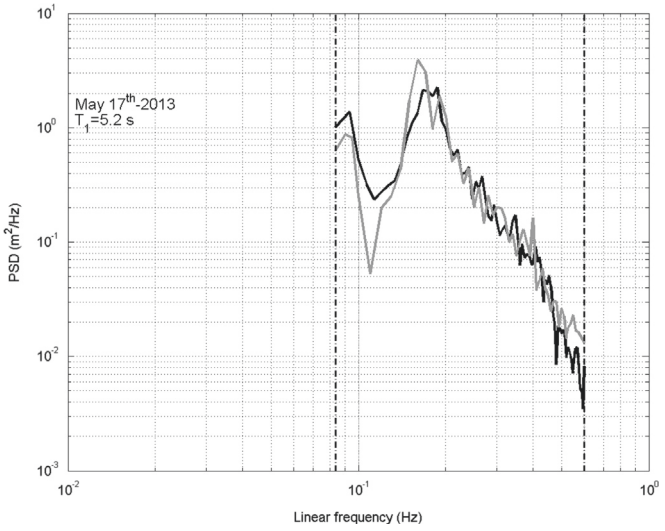

Fig. 6. Same as in Fig. 5 but for May 17th.

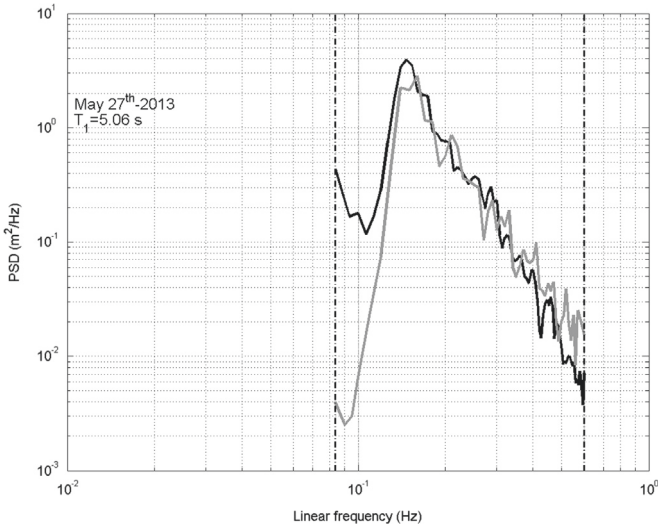

Fig. 7. Same as in Fig. 5 but for May 27th.

Table 2
SSignificant wave height (H_s), mean period (T_1), zero up-cross periods (T_2) and peak period (T_p) measured from glider and the Datawell Waverider Mk3.

Date	Parameter	Glider	Waverider	Difference (%)
March 7th	H_s (m)	1.02	1.19	14.2
	T_1 (s)	6.03	6.04	0.16
	T_2 (s)	5.38	5.37	0.18
	T_p (s)	9.37	8.33	12.5
May 17th	H_s (m)	1.67	1.8	7.2
	T_1 (s)	5.17	5.2	0.6
	T_2 (s)	4.8	4.85	1.0
	T_p (s)	6.06	6.17	1.8
May 27th	H_s (m)	1.81	1.6	13.1
	T_1 (s)	5.52	5.06	9.0
	T_2 (s)	5.20	4.72	8.0
	T_p (s)	6.8	6.57	3.5

3.3. Validation of directional spectra derived from surfaced glider responses

Although the scope of the present study was focused on non-directional properties of the sea state, accelerations collected by the sensor package PhidgetSpatial 3/3/3 and magnetic fluxes measured by the glider compass were employed to investigate the directional wave spectrum. Magnetic fluxes from the Phidget-Spatial 3/3/3 were discarded as no calibration procedure of its compass chips was followed. The directional wave spectrum $S(f,\theta)$ (f being the frequency and θ the direction of propagation) determines the way the energy of surface waves is distributed in frequencies and direction of propagation. In the framework of linear wave theory and by assuming a random phase distribution among the various components, the following mathematical relationship is obtained between $S(f,\theta)$ and the cross-spectra $G_{\alpha\beta}(f)$ of two signals α and β recorded simultaneously at the same location (Benoit et al., 1997):

$$G_{\alpha\beta}(f) = \int_0^{2\pi} H_\alpha(f,\theta) H^*_\beta(f,\theta) S(f,\theta) d\theta \tag{14}$$

where $H_\alpha(f,\theta)$ is now the transfer function between the surface elevation and any other wave signal α and the superscript $*$ stands for the complex conjugate. The directional spectrum could be determined uniquely from the cross-spectra of an infinite number of wave signals. This is not the case in reality as the number of wave signals recorded by measuring devices is finite, therefore, additional assumptions need to be considered to compute the directional spectrum. Different methods have been proposed in the literature to accomplish the inversion of Eq. (14). Among them, this work makes use of the Extended Maximum Entropy Principle (EMEP), proposed by Hashimoto (1997) and implemented in Matlab in the DIWASP (2012), to determine $S(f,\theta)$ from Eq. (14). Heave, surge and sway glider motions were used as wave signals. A whole set of informative directional parameters are easily derived once the directional wave spectrum is estimated. The present work is limited to the analysis of the direction and directional spread at the peak period, because these were the only directional information collected from the Datawell Waverider Mk3 during the glider deployments. Table 3 displays the compass bearings and directional spreads of the peak period estimated from the glider accelerations and the waverider. Directional information is provided in nautical convention, *i.e.*, the direction the waves are coming from. Unfortunately, no compass information from the glider was recorded during March 7th, preventing the reference of the directional wave spectra to an Earth coordinate system in this deployment.

Results show an agreement between the directions of the peak period derived from the glider and the waverider. More significant deviations are found for the directional spread of the wave direction at the peak period. While limited by an experimental design focused on the estimation of non-directional wave parameters from glider motions, these results provide robust indications that the directional wave spectrum can also be estimated from the motions of a surfaced glider. Further field tests would be required to reinforce the results presented in this sub-section.

Table 3
Direction (D_p) and directional spread (σ_p) at peak period measured from glider and the Datawell Waverider Mk3.

Date	Parameter	Glider	Waverider	Difference (%)
May 17th	D_p (°)	259	232	11.6
	σ_p (°)	50	40	25
May 27th	D_p (°)	236	234	0.8
	σ_p (°)	55	45	22.2

4. Discussion and conclusion

Underwater gliders provide the possibility to sample wide ocean areas in a sustained way. Presently, temperature and salinity are the ocean variables most commonly gathered from glider platforms. However, it is envisioned that these platforms could provide information about a wider range of environmental parameters. Sea state condition is among them. This could be achieved by expanding glider sensing capabilities to include an accelerometer package to determine the platform motions when excited by ocean waves.

Determination of the response of a surfaced Slocum glider platform to regular wave is a requirement to infer sea state conditions from the platform motions. This can be achieved by direct measurements or by numerical computations. In this study, the transfer functions of a glider at sea surface have been determined assuming small departures from the equilibrium position at the sea surface of an homogeneous, irrotational and inviscid fluid. The effects of viscosity are significant in seakeeping for roll and yaw motions due to periodic boundary layer separation (Bertram, 2011). However, they are expected to be negligible for heave, surge and sway motions when a body closely follows the sea surface. This is hypothesized on the basis of the small velocities of the body relative to the fluid. The assumption of irrotational flow naturally derives from the inviscid situation, because rotational components of the velocity field are usually generated at the hull as a consequence of the existence of viscosity (viscous resistence). Dynamical nonlinearities need to be considered when the wave phenomena is inherently nonlinear (shallow water waves, $\tanh(kD) < 0.3$) or under extreme motions (*e.g.*, capsizing). Experimental determination is probably required to infer the dynamical response of the glider under these conditions.

Numerical results indicate that the heave response function of a Slocum glider is a real number close to one for wave periods longer than 6 s. Then, the effects by the geometry and inertia of the body and the incidence of the wave on the platform response in heave can be neglected. The surfaced glider follows the sea surface and the waverider buoy analogy holds, making the estimation procedure relatively inexpensive in terms of computing demand. This would facilitate the processing on board the glider platform with an adequate modification of the protocols activated when the platform surfaces.

Resonances in heave are expected to occur in a surfaced Slocum glider. In the present case, a resonant peak was found at about 5 s, which has been identified as the natural period of the buoyant body. Notice that the natural resonance period depends on the hydrostatic restoring terms of the glider. The stern of Slocum

gliders is an open hull and buoyancy is provided by the inflation of a bladder. This could require a more accurate determination of the heave restoring term than determined here, which modelled the glider hull as a unit without open portions.

Response functions of surge and sway were also numerically computed. These are required to analyse the validity of the waverider buoy analogy when estimating directional wave properties. Unlike heave, response functions for surge and sway show a dependence on the direction of incidence of the wave field. This fact justifies the use of the heave, instead surge and sway, to estimate non-directional wave spectra. The lack (presence) of a resonant behaviour in sway response function of sway (surge) is another interesting feature derived from the results. This can be understood in terms of the dynamics of the surfaced glider. In essence, Eq. (1) encodes the dynamics of a damped and forced harmonic oscillator which restoring term is different from zero only for heave and pitch. These restoring coefficients are related to the force and torque generated by buoyancy and gravity. Consequently, natural frequency and resonance are mostly associated to heave and pitch oscillations. Resonant behaviour propagates to surge due to its inertial coupling with the pitch mode. Instead, glider natural frequency does not affect sway as this mode is dynamically uncoupled from heave and pitch.

An experimental program was conducted to determine the extend to which sea state conditions could be derived from the responses of a surfaced Slocum glider under the waverider buoy analogy. The experimental work was not exempted of difficulties due to the need to harmonize experimental needs with navigation safety conditions (glider deployments were done from a rubber boat). This limited the range of sea height conditions explored during the experiments.

Regarding non-directional parameters, experimental conditions justified the use of the waverider buoy analogy as determined from the analysis of the response function. Results show an excellent agreement between the estimates obtained from glider vertical accelerations and the ground truth values provided by a waverider. Agreement between glider estimates and waverider records, has also been found when estimating the wave direction from the glider motions and assuming the waverider buoy analogy. However, the directional spread obtained from gliders is significantly larger than that reported from the waverider. The origin of such discrepancy still remains unknown, but it is hypothesized that could be related to the impact of the glider geometry which substantially differs from the optimal one for this purpose (spherical geometry). While results are encouraging, further field experimentation would be required to confirm the findings regarding directional wave properties.

These results complement and extend the findings reported by Pereira and Sukhatme (2010), reinforcing the hypothesis that parameters of the sea state conditions could also be achieved from glider platforms when they are at surface. Gliders have not been specifically designed to monitor sea state conditions, but for other observational purposes. Still, they could offer, as an added value of their missions, a nice complement to observations of sea state conditions. Characterizing surface waves with gliders is not exempted of limitations. During a regular glider mission, the temporal coverage of the sea state estimates is coarser than for waverider buoys, as it is limited by the surfacing time programmed to satisfy the requirements of their main observational scope (monitoring the ocean's interior). However, gliders could offer a chance to enhance the spatial resolution of *in situ* sea state observations due to their manoeuvrability and facility to relocate in marine regions. Besides, glider observations are rapidly transitioning from platform-based to networks increasing the spatial coverage of ocean observations (Alvarez and Mourre, 2012; Alvarez et al., 2013).

To conclude, this work has investigated the applicability of the waverider buoy analogy to estimate non-directional and directional wave spectra from surfaced Slocum gliders. While the results are platform dependent, the approach developed can be easily generalized to other vehicles. This implies to determine, by numerical and/or experimental means, the response functions of the vehicle for different wave frequencies and directionalities. The long wave limit is then identified as that range of frequencies where the response functions are close to one. Platform signals are then trivially connected to wave signals and standard processing for wave spectra is applied.

For the particular case of surfaced Slocum gliders, the waverider buoy analogy is expected to work satisfactorily in most cases for wave periods bigger than 6 s for the Slocum glider. Deviations from reality are expected when the glider surfaces in wave patterns with a shorter time period due to the existence of a natural period of resonance. An accurate characterization of the glider response function for the different dynamical degrees of freedom would then be needed in order to relate the surfaced glider response to the sea wave spectrum. Nevertheless it is important to highlight that the particular glider geometry may degrade the estimation of some directional properties.

Acknowledgments

This work has been partially funded by the NATO-Allied Command Transformation-ACT and the EU project FP7- INFRASTRUCTURES-2011-1 "Gliders for research, ocean observation and management-GROOM" under grant agreement n.284321 GROOM.

References

AlpersW., Ocean surface wave imaging from Seasat to Envisat. In: Proceedings 2003 IEEE International Geoscience and Remote Sensing Symposium, 2003. IGARSS "03, 1, pp. 35-37.

Alvarez, A., 2010. Redesigning the SLOCUM glider for torpedo tube launching. IEEE J. Oceanic Eng. 35 (4), 984–991.

Alvarez, A., Mourre, B., 2012. Oceanographic field estimates from remote sensing and glider fleets. J. Atmos. Oceanic Technol. 29 (11), 1657–1662. http://dx.doi.org/10.1175/JTECH-D-12-00015.1.

Alvarez A., 2012. Transfer Functions of an Underwater Glider at Sea Surface: Numerical Computation—La Spezia: CMRE, 2012/11. (Monographs; CMRE Memorandum Report (MR series) CMRE-MR-2012-002—NATO Unclassified.

Alvarez, A., Chiggiato, J., Schroeder, K., 2013. Mapping sub-surface geostrophic currents from altimetry and a fleet of gliders. Deep Sea Res. Part I: Oceanogr. Res. Pap. 74, 115–129. http://dx.doi.org/10.1016/j.dsr.2012.10.014.

Benoit M., Frigaard P., Schaffer H.A., 1997. Analysis of multidirectional wave spectra: a tentative classification of available methods. In: Proc. IAHR Seminar on Multidirectional Waves and their Interaction with Structures 27th IAHR Congress (San Francisco), pp. 159-182.

Bertram, V., 2011. Practical Ship hydrodynamics. Butterworth-Heinemann p. 390.

Bezgodov, A., Esin, D., 2014. Complex network modeling for maritime search and rescue operations. Proc. Comp. Sci. 29, 2325–2335.

Chen-Tung, A.C., 2009. Nihoul, J.C.J., Chen-Tung, A.C. (Eds.), Field Measurement, in Oceanography: v3. EOLSS Publishers Co Ltd., p. 378.

D'Asaro, E.A., Thomson, J., Shcherbina, A.Y., Harcourt, R.R., Cronin, M.F., Hemer, M. A., Fox-Kemper, B., 2013. Quantifying upper ocean turbulence driven by surface waves. Geophys. Res. Lett. 41, 1–6.

Datawell B.V., Datawell Waverider Reference Manual, 2006, http://www.datawell.nl/Support/Documentation/manuals.aspx.

DIWASP, A Directional Wave Spectra Toolbox for MATLAB®: User Manual. Research Report WP-1601-DJ (V1.1), 2012, Centre for Water Research, University of Western Australia.

Earle, M.D., 1996. Nondirectional and directional wave data analysis procedures, NDBC technical document 96-01. NOAA, 37.

Graber, H.C., Heron, M.L., 1997. Wave height measurements from HF radars. Oceanography 10, 90–92.

Goda, Y., 2010. Random Seas and Design of Maritime Structures. World Scientific Publishing Company p. 732.

Goodman, L., Levine, E.R., Wang, Z., 2010. Subsurface observations of surface waves from an autonomous underwater vehicle,. IEEE J. Oceanic Eng. 35 (4), 779–784.

Hashimoto, N., 1997. Analysis of the directional wave spectrum from field data. Adv. Coastal Ocean Eng. 3, 103–143.

Heimbach, P., Hasselmann, S., Hasselmann, K., 1998. Statistical analysis and intercomparison of WAM model data with global ERS-1 SAR wave mode spectral retrievals over 3 years. J. Geophys. Res. 103, 7931–7977.
Holthuijsen, L.H., 2010. Waves in Oceanic and Coastal Waters. Cambridge University Press p. 404.
Hsu, T.-J., Elgar, S., Guza, R.T., 2006. Wave-induced sediment transport and onshore sandbar migration. Coastal Eng. 53, 817–824.
Hwang, P.A., Wang, D.W., Walsh, E.J., Krabill, W.B., Swift, R.N., 2000. Airborne measurements of the wavenumber spectra of ocean surface waves. Part I: Spectral slope and dimensionless spectral coefficients. J. Phys. Oceanogr. 30, 2754–2767.
ITTC, Report of the seakeeping committee. In: The Proceedings of the 17th International Towing Tank Conference ITTC84, 1984,8-15 September, Goteborg, Sweden.
Kanevsky, M.B., 2009. Radar Imaging of the Ocean Waves. Elsevier, Amsterdam p. 208.
Komar, P.D., 1998. Beach Processes and Sedimentation. Prentice Hall, New Jersey p. 544.
Lee, C.H., Newman, J.N., 2004. "Computation of wave effects using the panel method," in Numerical models in fluid–structure interaction. In: Chakrabarti, S.K. (Ed.), Numerical Models in Fluid–Structure Interaction. WIT Press, Southampton, UK, pp. 41–81.
Lee, C.H., Scalvounonos, P.D., 1989. Removing the irregular frequencies from integral equations in wave-body interactions. J. Fluid Mech. 207, 393–418.
Lenain, L., Melville, W.K., 2014. Autonomous Surface Vehicle Measurements of the Ocean's Response to Tropical Cyclone Freda. J. Atmos. Ocean. Tech, 2169–2190.
Queffeulou, P., 1987. SEASAT wave height measurement: a comparison with sea-truth data and wave forecasting model-Application to the geographic distribution of strong sea states in storms. J. Geophys. Res. 88, 1779–1788.
Newman, J.N., 1977. Marine Hydrodynamics. The MIT Press p. 424.
Niclasen, B.A., Simonsen, K., 2007. Note on wave parameters from moored wave buoys. Appl. Ocean Res. 29, 231–238.
Pereira, A.A., Sukhatme, G.S. (2010), Estimation of Wave Parameters from Accelerometry to Aid AUV-shore Communication, OCEANS 2010 IEEE, 24-27 May 2010, Sydney, 10.1109/OCEANSSYD.2010.5603792.
Reineman, B.D., Lenain, L., Castel, D., Melville, W.K., 2009. A portable airborne scanning lidar system for ocean and coastal applications. J. Atmos. Oceanic Technol. 26, 2026–2041.
Romero, L., Melville, W.K., 2010. Airborne observations of fetch-limited waves in the Gulf of Tehuantepec. J. Phys. Oceanogr. 40, 441–465.
Shapiro, A.D., 2010. Available. Remotely piloted underwater glider crosses the Atlantic. IEEE Spectr..
Stommel, H., 1989. The Slocum mission. Oceanography 2, 22–25.
Sullivan, P.P., McWilliams, J.C., 2010. Dynamics of winds and currents coupled to surface waves. Ann. Rev. Fluid Mech. 42, 19–42.
Sutherland, G., Ward, B., Christensen, K.H., 2013. Wave-turbulence scaling in the ocean mixed layer. Ocean Sci. 9, 597–608.
Swift, C.T., Wilson, L.R., 1979. Synthetic aperture imaging of ocean waves. IEEE Trans. Antennas Propag. 27, 725–729.
Tesle, J.G., Noblesse, F., 1986. Numerical evaluation of the Green function of water-wave radiation and diffraction. J. Ship Res. 30, 69–84.
Testor, P., Meyers, G., Pattiaratchi, C., Bachmayer, R., Hayes, D., Pouliquen, S., Petit de la Villeon, L., Carval, T., Ganachaud, A., Gourdeau, L., Mortier, L., Claustre, H., Taillandier, V., Lherminier, P., Terre, T., Visbeck, M., Karstensen, J., Krahman, G., Alvarez, A., Rixen, M., Poulain, P., Osterhus, S., Tintore, J., Ruiz, S., Garau, B., Smeed, D., Griffiths, G., Merckelbach, L., Sherwin, T., Schmid, C., Barth, J., Schofield, O., Glenn, S., Kohut, J., Perry, M., Eriksen, C., Send, U., Davis, R., Rudnick, D., Sherman, J., Jones, C., Webb, D., Lee, C., Owens, B., 2009. Gliders as a component of future observing systems. In: Hall, J., Harrison, D.E., Stammer, D. (Eds.), Proceedings of OceanObs'09: Sustained Ocean Observations and Information for Society, vol. 2. ESA Publication, Venice, Italyhttp://dx.doi.org/10.5270/OceanObs09.cwp.89 21-25 September 2009,.
Tucker, M.J., Pitt, E.G., 2001. Waves in Ocean Engineering, Elsevier Ocean Engineering Book Series, 5. Elsevier p. 521.
Vanem, E., Bitner-Gregersen, E.M., 2012. Stochastic modelling of long-term trends in the wave climate and its potential impact on ship structural loads. Appl. Ocean Res. 37, 235–248.
Webb, D.C., Simonetti, P.J., Jones, C.P., 2001. Slocum: an underwater glider propelled by environmental energy. IEEE J. Oceanic Eng. 26, 447–452.
Wehausen, J.V., Laitone, E.V., 1960. Surface Waves. In: Flügge, S., Truesdell, C. (Eds.), Encyclopaedia of Physics, 9. Springer Verlag, pp. 446–778.
Wolf, J., Prandle, D., 1999. Some observations of wave-current interaction. Coast. Eng 37 (3), 471–485.
Young, I.R., 1999. Wind Generated Ocean Waves. Elsevier p. 287.
Yu, J., 2006. On the instability leading to rip currents due to wave–current interaction. J. Fluid Mech. 549, 403–428.

Document Data Sheet

Security Classification		Project No.
Document Serial No.	**Date of Issue**	**Total Pages**
CMRE-PR-2019-104	June 2019	9 pp.

Author(s)

Alberto Alvarez

Title

Assessment of sea wave spectra using a surfaced glider

Abstract

The determination of non-directional and directional sea wave spectra is attempted by analysing the dynamical response of a surfaced Slocum glider. The method makes use of the glider heave motion to infer non-directional properties of the wave spectra. In addition, surge and sway motions are considered to derive wave directionality. The transfer functions for heave, surge and sway for a surfaced Slocum glider has been computed to determine the impact of the body geometry/inertia and the angle of incidence on the response of the surfaced platform when excited by regular waves. Numerical results show that for wave periods longer than 6 s, motions measured at the glider platform can be assumed equivalent to motions experimented by the water parcels at the sea surface. Spectral information about sea state conditions can then be directly derived from the measurement of glider responses. Results also reveal a natural period of the surfaced glider at around 5 s. A series of field experiments were conducted during March 7th, May 17th and May 27th of 2013 in a marine region off-shore La Spezia, to validate the methodology. Specifically, the wave spectra derived from a Slocum glider equipped with a set of accelerometers was compared against the values provided by a Datawell Waverider Mk3 moored in the vicinity of the glider deployment. Agreement has been found between the non-directional estimates from the glider and the values measured by the waverider. Regarding wave directionality, glider estimates of peak direction agree well with those reported by the waverider. More significant differences are found between the directional spread estimates.

Keywords

Underwater glider, response amplitude operator, waverider buoy analogy, accelerometer, non-directional and directional sea wave spectra

Issuing Organization

NATO Science and Technology Organization
Centre for Maritime Research and Experimentation

Viale San Bartolomeo 400, 19126 La Spezia, Italy

[From N. America:
STO CMRE
Unit 31318, Box 19, APO AE 09613-1318]

Tel: +39 0187 527 361
Fax:+39 0187 527 700

E-mail: library@cmre.nato.int